Cellular Magnesia/Carbon Refractories: Processing, (Thermo-)Mechanical Characterization and Finite Element Modeling

D. Foetz, D. Quinten, G. Falk, A. Jung, T. Bleistein, S. Diebels

Fabrication steps of MgO–C refractories with a cellular carbon structure are shown: First, the transformation of resin coated polyurethane foams into reticulated vitreous carbon, followed by the antioxidant coatings with zirconia or silicon carbide and then the infiltration with aqueous magnesia slurries. Samples were tested regarding their (thermo-)mechanical properties. In addition, their corrosion behaviour in an induction furnace was investigated. Finally, thermal damage after thermal shock of a standard MgO–C brick with randomly distributed carbon was compared with that of a MgO–C sample that contains carbon in a perfect periodic cellular structure by using the finite element analysis with a thermo elastic model.

1 Introduction

Carbon composites include a wide variety of materials with good qualities such as low density, high flexural and tensile strength, heat resistance, high oxidation and abrasion resistance, high tear resistance and excellent corrosion and thermal shock resistance. Because of all these properties carbon containing materials, especially combinations of carbon and magnesia, belong to the preferred refractories at the moment and certainly also in the future. However, even higher demands are made on the refractories of the next generation, as increased service life requires amongst others even higher thermal shock and corrosion resistivity [1].

In the steelmaking industry, refractory linings are subjected to quasi-static and dynamic thermal loading, which lead to thermal induced stresses. Permanent thermal stresses arise during quasi-static thermal loading in heterogeneous materials with different Coefficients of Thermal Expansion (CTE) of the constituents, whereas no gradient in temperature occurs. During dynamic thermal loading, also called thermal shock, the temperature is suddenly raised, causing large temperature gradients in the materials. These temperature gradients cause temporary thermal stresses in homogeneous and also heterogeneous materials. They disappear at temperature balance if the material is only linear-elastically deformed by the thermal stress. Both types of thermal induced stresses cause damage. Permanent thermal stresses cause thermal damage, which originates from the isotropic thermal expansion of constituents with a mismatch in the CTE. Damage from temporary thermal stresses occurs not only in heterogeneous but also in homogeneous materials. This elastic-driven damage is called mechanical damage [2, 3].

Cellular materials like periclase (MgO)-filled carbon foams [4–7] consist of different hierarchical construction levels. As a result, their behaviour could be modelled on the macro scale, under the assumption of a homogeneous component, or on the micro scale, where the complete microstructure consisting of different phases is taken into account. The modeling of MgO–C refractories is not only a multiphase but also a multiphysics issue, leading to thermomechanical coupled problems. Since the description of thermal shock and thermal shock parameters by Kingery [8] and Hasselman [9–11], different modeling approaches for thermal shock and transient thermomechanical damage in refractory materials have been developed.

First stage computational models were based on linear elastic fracture mechanics. In a second step, there was the incorporation of phenomenological crack models for quasi-brittle materials [12, 13]. More recent models [14–17] suggest a multiplicative split for the two types of thermal induced stresses and damage. According to the assumption that both damage mechanisms act independently on different scales, Damhof et al. developed a non-local thermal shock damage model with an additive combination of elastic-based damage and thermal damage [2, 3, 18]. The elastic damage is connected to the macro scale causing elastic strains due to temperature gradients that lead to internally and externally constrained thermal expansion. The thermal damage

D. Foetz, D. Quinten, G. Falk
Saarland University, Research Group Structural and Functional Ceramics
Campus C6 3
66123 Saarbrücken
Germany

A. Jung, T. Bleistein, S. Diebels
Saarland University, Institute of Applied Mechanics, Campus A4 2
66123 Saarbrücken
Germany

Corresponding author: *D. Foetz*
E-mail: d.foetz@nanotech.uni-saarland.de

Keywords: reticulated vitreous carbon, thermal shock, FEM modeling

Received: 01.12.2015
Accepted: 07.01.2016

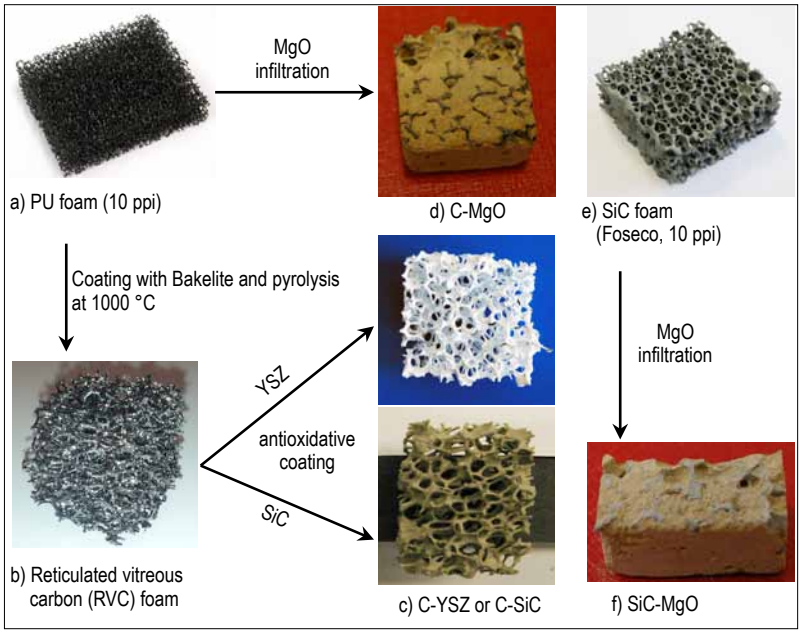

Fig. 1 Processing steps

caused by isotropic thermal expansion due to homogeneous temperature changes acts on the micro scale as a result of the difference in the CTE between the constituents.

MgO–C materials are well-established in the steel making industry. Magnesia has a high melting point, but shows poor thermal shock resistivity. This is due to the high CTE, that leads to high temporary thermal stresses. When carbon is added, it compensates this drawback as its good thermal conductivity leads to a rapid reduction of thermal gradients [19]. For this positive effect to occur, the carbon has to form a three dimensional network. For the production of MgO–C bricks, it is state of the art to mix the dry components and press them to their final shape. In this fabrication process carbon must not be added below a certain concentration limit. Otherwise, the carbon phase is not interconnected and the thermal conduction is blocked.

A reduction of carbon is interesting for two reasons: The first one is the possibility to use bricks with low carbon content also in the production process of high-quality, high alloyed steel, as the steel would otherwise be carburized. The second reason is that less carbon can be oxidized to CO or CO_2, which pollute the environment. The latter is one of the key challenges of the priority program DFG-SPP 1418 Refractories-Initiative to Reduce Emission – FIRE. One possibility to reduce the carbon content without losing its good effects is to introduce the carbon in terms of carbon foam [20, 21]. To further lower the emissions, a protection layer can be coated onto the carbon, which protects it from oxidation [22]. The cellular carbon foams are made for example of coal tar or petroleum-based pitches [23–25]. Another possibility is the use of synthetic resins such as Novolak and Resole [26–29]. They can be used for the replica technique, where a polymer foam is coated with resin and afterwards pyrolized, leading to a reticulated vitreous carbon [30, 31].

When working with magnesia, hydration problems must not be neglected. As air humidity is already critical, the usage of aqueous slurries poses an even bigger challenge. However, literature presents some approaches [32–34].

2 Experimental description

2.1 Materials and sample preparation

2.1.1 Carbon foam synthesis and processing

The Reticulated Vitreous Carbon (RVC) foams are made via the replica technique. Starting material of all samples is polyurethane (PU) foam with a pore size of 10 ppi (ISP GmbH/DE; Fig. 1a). In the first step, Novolak resin powder (Bakelite PF 0227 SP 01, Momentive Specialty Chemicals GmbH/DE) was mixed on a magnetic stirrer half-and-half with ethanol. The PU foam was then immersed into this mixture. By compression and rolling of the sponges, the excess slurry was removed and the samples were left to dry in a drying chamber at 60 °C for 72 h. The following heat treatment was performed in an electric tubular furnace with argon atmosphere. The final pyrolysis temperature of 1000 °C was reached with a heating rate of 2 K/min and kept for 2 h. During this procedure the PU foam and the Novolak resin transformed into a glassy carbon phase. The samples are now referred to as RVC (Fig. 1b). The transformation process was analysed thermogravimetrically (STA409, Netzsch GmbH/DE) in a nitrogen atmosphere and at a heating rate of 10 K/min. The resulting foams were examined in a scanning electron microscope.

2.1.2 Antioxidant coating of carbon foam

In the second step, the RVC foams were supplied with an antioxidant coating of Yttrium-Stabilized Zirconia (YSZ) and Silicon Carbide (SiC), respectively. To successfully prevent the carbon foam from reacting with oxygen, the coating has to has a sufficient thickness. For that reason, κ-carrageen (Ceamgel M 9310, Ceamsa/ES) was used as a gelling additive. Water and carrageen were mixed and heated up to 75 °C, completely dissolving the carrageen.

The YSZ (TZ-8Y, TOSOH/JP) and Antiprex A40 (BASF/DE) as dispersing agents were mixed in water and heated up to 45 °C. The two mixtures were then poured together, so that the final suspension reached a temperature of about 55 °C and consisted of about 60 mass-% of YSZ, 1,3 mass-% of carrageen, and 1,33 mass-% of Antiprex A40. For the SiC coatings, a slurry of 60 mass-% SiC, 1,3 mass-% carrageen and NaOH for pH adjustment was mixed in one step and heated up to 65 °C. Finally the RVC foams were dipped into the particular slurry and treated with an airstream in order to remove the films that closed the cell structure of the foams. Where necessary, the dipping process was repeated to reach the desired coating thickness.

2.1.3 Processing of MgO–C

To prevent magnesia from hydrating in the aqueous slurry, a recipe according to [34] was used. Thereto 70 mass-% of magne-

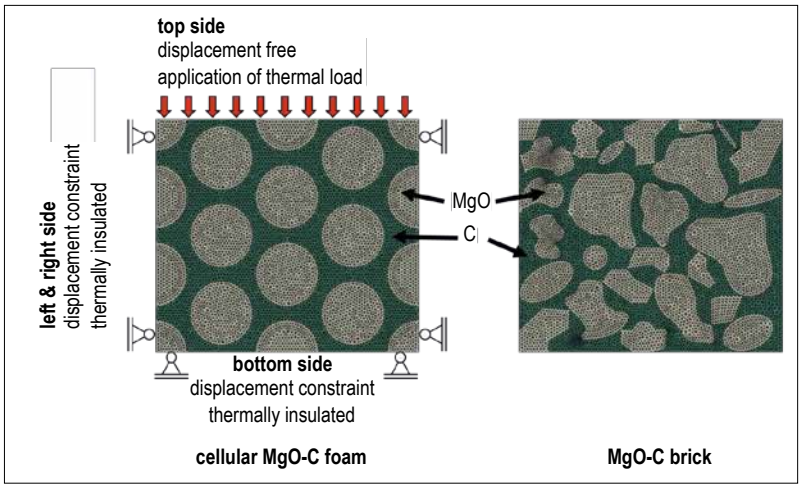

Fig. 2 RVE microstructure of the MgO–C foam including the applied boundary conditions (l.), and the RVE microstructure of the common MgO–C brick (r.)

sia (TA-3, Lehmann & Voss & Co./DE) was mixed with 0,4 mass-% Dolapix CE 64 (Zschimmer & Schwarz/DE), 0,4 mass-% Darvan 7-N (Vanderbilt Minerals LLC/US) and 0,4 mass-% sodium lignin sulfonate N18 (Otto Dille, Baeck GmbH & Co. KG/DE) into water. The infiltration of the foams with the MgO slurry was supported by shaking the silicone moulds on a vibrating plate.

To compare the fabricated samples, further referred to as lab samples, a commercially available refractory brick (Macarbon L710 F, Refratechnik Steel GmbH/DE), further referred to as reference sample, was also included in the testing.

2.2 Mechanical characterization

As both reference samples and lab samples are very sensitive to humidity, it was only possible to dry cut them into the appropriate dimensions for mechanical testing. Unfortunately, the final sizes differed too much from those given in the particular standardized procedures, so that all measurements only were driven based on the following rules.

The procedure to determine the Hot Modulus of Rupture (HMOR) is described in DIN EN 993-7. The bars with rectangular cross section were around 150 mm × 20 mm × 20 mm in dimensions. The applied loading rates in the testing machine were chosen to 0,15 MPa/s for the reference samples and 0,02 MPa/s for the lab samples. Heating up with 300 K/h, the test temperature of 1000 °C was held for 1 h. The whole setup was kept under argon atmosphere.

The measurement of the Modulus of Rupture (MOR) for refractories is specified in DIN EN 993-6. The bars with rectangular cross section were about 150 mm × 20 mm × 20 mm in dimensions. The forces applied to this samples were measured until failure occurred.

The Cold Crushing Strength (CCS) of the cubed samples was measured according to DIN EN 993-5 at room temperature.

2.3 Thermomechanical characterization

The reference and the lab samples were both tested in an induction furnace assembly with regard to their behaviour in contact with iron slag. For that purpose, steel in an alumina crucible was heated up to 1600 °C. The samples were then positioned close above the melt, where they were heated up by the thermal radiation of the hot liquor. When the samples reached 1100 °C, the melt was further heated up to 1700 °C and 500 g of slag were added. Finally the samples were dipped into the hot melt for several minutes. For characterization purposes the samples were dry cut into several sections. As the MgO–SiC laboratory sample was very fragile, it was embedded into a plastic resin, which made grinding possible. The segments were examined in the SEM in regard to their structure and their chemical composition.

3 Modeling

In the present contribution, the randomly distributed microstructure of a common MgO–C brick is compared with the regular, periodic microstructure of the new cellular MgO–C foams with respect to their thermal shock behaviour. Similar to the early stages in thermomechanical modeling of refractories, a linear elastic computational approach is used. Therefore, a 2D model of both microstructures of MgO–C refractories is simulated by linear thermoelasticity, using a transient and static coupled temperature-displacement finite element analysis in Abaqus™. The failure stresses in both, conventional MgO–C brick and new MgO–C hybrid foam, are evaluated to analyse the structure-property relation. The maximal occurring tensile stresses are used as failure criteria. Therefore, the assumption was made that the carbon and the periclase phase remain linear elastic in the analysed temperature region. The MgO–C foam consists of a carbon matrix with periodically distributed circular pores filled with MgO. For the MgO–C bricks, irregular shaped inclusions of MgO are distributed in the matrix. Both, foam and brick, contain 62 % of MgO and 38 % of C. A rectangular reference Representative Volume Element (RVE) of 20 mm × 18 mm (width × height) was built for the investigation of the thermal shock behaviour for each microstructure. The RVE structures are stress-free at ambient temperature and the models are meshed by triangular first order plain-strain shell elements (CPE3T). In order to simulate a segment of a larger part of a refractory material, which is thermally loaded on the top side, and to prevent rigid body motion, a Dirichlet boundary condition is applied on the left, right, and bottom sides of the RVE by a constrained displacement of the boundary nodes in the normal direction of the three sides and is thermally insulated, whereas the displacement of the top boundary nodes is free and thermal loading is applied on the top boundary nodes. Fig. 2 outlines both investigated structures and the applied boundary conditions for the MgO–C foam.

From the top side, in the first step both microstructures were quasi-statically heated from ambient temperature to 1300 °C (1573 K) within 7200 s. In a second step, a thermal shock of 500 °C up to a temperature of 1800 °C (2073 K) is applied. This two-step procedure is similar to the treatment in the steelmaking industry. In order to reduce the thermally induced stresses and failure, the ladles will be quasi-statically heated before pouring molten steel of about 1800 °C (2073 K) in the second step into the ladle.

For simplification of the model, the material parameters are assumed to be tempera-

ture independent. The chosen parameters for carbon and periclase are outlined in Tab. 1. The CTE of carbon is one order of magnitude lower than that of periclase. As a result of this difference in the CTE, during the Thermal Shock (TS) experiments, failure in both investigated MgO–C refractories occurs by thermal and by elastic mechanical damage. In order to investigate the effect of air pores in the microstructure, in a second numerical investigation, the same microstructures extended by a third phase, air, are investigated. This leads to the following material contents: 52 % MgO, 38 % C, and 10 % air. For all investigated microstructures, the contents of the periclase phase, the carbon phase and the air are equal in the foam and the brick.

4 Results and discussion

4.1 Carbon foam synthesis

The results of the thermogravimetric analysis of the polyurethane foam and the bakelite resin are shown in Fig. 3. The bakelite loses a total of 45,7 % of its original mass, whereas the PU foam is almost completely decomposed at temperatures >420 °C. At the final temperature only 2,2 % of the original mass of the PU foam are left.

That leads to a structure shown in Fig. 4, where the transformed bakelite builds up a reticulated vitreous carbon foam. Because of the almost complete pyrolysis of the polyurethane, the struts are hollow. This results in a pretty fragile design. In addition, the heating rate of 2 K/min still seems to be a bit too high, as a lot of bubbles are visible. This also reduces the strength of the RVC foam and makes the handling of the foams rather difficult.

4.2 Antioxidant coating of carbon foam

With the described procedure, it was possible to deposit the antioxidant coatings in a rather homogeneous way onto the RVC foams. Fig. 5 shows two samples that were coated with YSZ. There are only a few smaller pores in the structure that are completely closed by YSZ films. With the air treatment right after the coating, it is possible to keep most of the pores open.

The rheological properties of SiC or YSZ slurries containing carrageen as gelling additive are shown in Fig. 6. When heated up and subsequently cooled down, both suspensions reach the gelling point at a temperature of about 30 °C.

The steep increase of viscosity during further cooling allows for coating of the RVC foams with relatively thick antioxidant films. A SEM image of a RVC strut coated with zirconia is shown in Fig. 7. The hollow core of the RVC strut, the bubbles in the RVC, and the coating are visible. It is also clearly evident that the coating is very thin at the edges of the struts, which is a typical problem of dip coating processes.

4.3 Processing of MgO–C

Using the described recipe, it was possible to get pourable slurries of 75 mass-% magnesia in water. A problem that occurred was the shrinkage of the monolithic samples, which led to huge cavities, see Fig. 8 a. By repeatedly casting layers and drying them before casting the next layer, a dense structure without big pores was achieved,

Tab. 1 Material parameters for reticulated vitreous carbon (RVC) and periclase [30, 35, 36]

	RVC (C)	Periclase (MgO)
Density [kg/m^{-3}]	1450	3580
Young's modulus [GPa]	35	270
Poisson ratio	0,23	0,17
CTE [10^{-6} K^{-1}]	2,5	12
Thermal conductivity [W K^{-1} m^{-1}]	5	30
Specific heat capacity [J K^{-1} kg^{-1}]	709	1001
Compression strength [MPa]	580000	2600
Tensile strength [MPa]	260	220

Fig. 8b. As the RVC foams after the pyrolysis were very fragile, further experiments concerning the MgO infiltration were initially performed with the original PU foams. The problem now was that the MgO slurry had to penetrate into the pores of the foam. In Fig. 9 the viscosities of two MgO slurries with varying solid content are shown.

As the viscosity is decreased significantly by reducing the MgO content from 75 – 70 mass-%, this slurry was chosen for the infiltration process. But nevertheless, Fig. 8c shows that the magnesia still does not enter all of the pores and that a lot of cavities appear in the sample. The viscosity curve shows a distinct shear thinning behaviour. This was used and the samples were shaken during the infiltration process, resulting in samples like the one in Fig. 8d, with the PU foam structure completely filled with MgO and no cavities visible. As the RVC foams were very brittle and rather difficult to handle, further magnesia infiltration experiments were

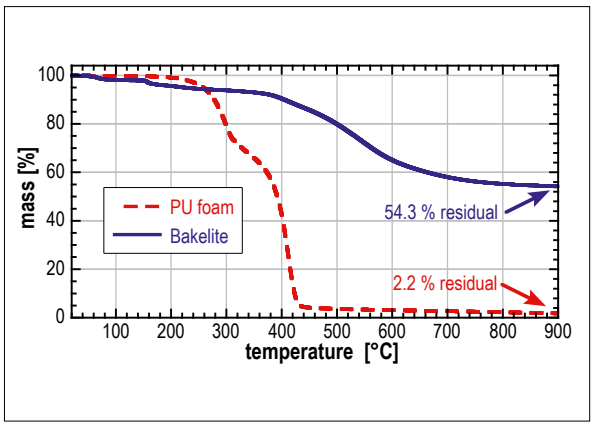

Fig. 3 Thermogravimetric analysis of the polyurethane foam and the Bakelite resin

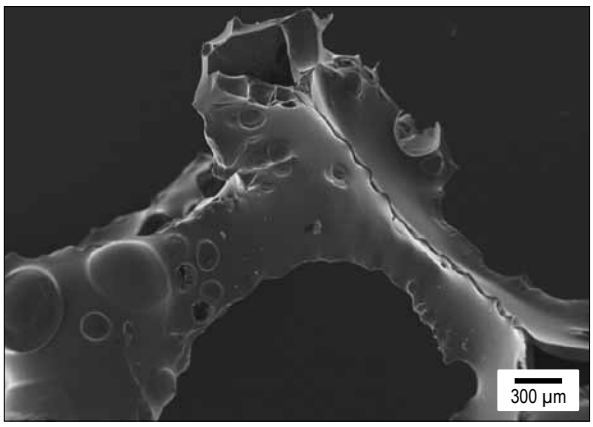

Fig. 4 SEM image of a strut of RVC foam pyrolized at 1000 °C

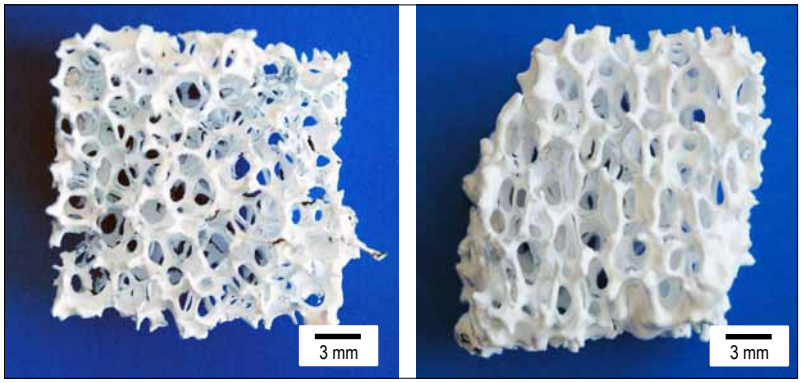

Fig. 5 Two examples for RVC foams coated with YSZ (green body)

carried out, using commercially available SiC foams. Fig. 1 f shows such a sample. In spite of shaking the samples during the magnesia infiltration, the formation of some cavities could not have been prevented.

4.3.1 (Thermo-)mechanical characterization

Tab. 2 displays the measured values in the mechanical testing. It can clearly be seen that the laboratory samples are in all measurements inferior to the reference samples. This can be explained by the rather loose

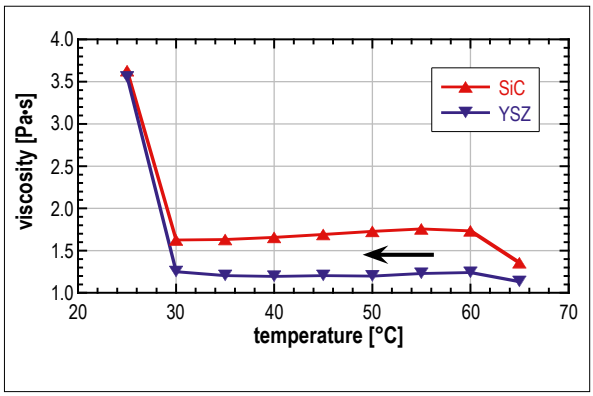

Fig. 6 Viscosities of antioxidant slurries containing carrageen as gelling additive

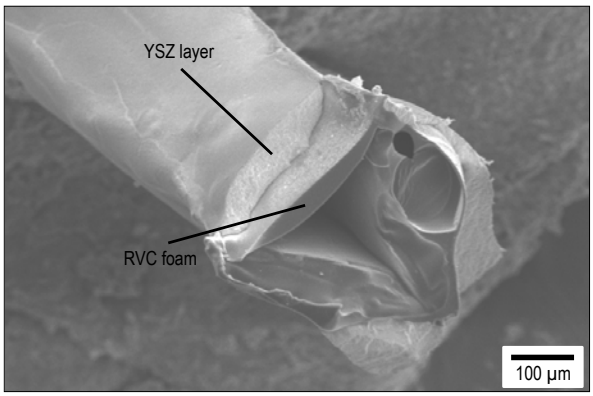

Fig. 7 SEM image of a reticulated vitreous carbon foam coated with yttrium-stabilized zirconia (green body)

Fig. 8a–d Development steps passed during casting of MgO slurries: a) shrinkage during drying; b) optimized layer by layer casting; c) pores after infiltration into the PU foam; and d) improvement by additional shaking

bonding of the magnesia grains with each other and with the silica foam. In contrast to this, the reference sample provides a dense packed structure with good interconnectivity between the components. Additionally, the values for the reference sample obtained during previous investigations are specified [4]. The term "aged" is added, as the samples were stored for a while before testing without protection against humidity. This led to the conversion of magnesia into magnesium hydroxide, resulting in a degradation of the mechanical properties, as shown by the much lower values listed in the table. Based on this experience, all samples, laboratory and reference ones alike, were only stored after being sealed in plastic foil.

4.3.2 Thermomechanical characterization

Pictures of the samples and their cross sections after the corrosion testing are shown in Fig. 10–11. Each sample was hung into the device with the right side up. So cross section 1) refers to the material that has been exposed to a temperature of at least

1100 °C, but was not in contact with the slag. Looking at the cross sections of the reference sample in Fig. 10, no greater changes of structure are visibly detectable. This is proven by Fig. 12a, where the composition of the reference sample in section 2) is given in an EDX line scan. The silicon and the calcium, the latter being the slag, penetrated only about 1 mm into the sample. After that the carbon shows the average concentration of 10 mass-%, which is the given value from the manufacturer. At about 3 mm the carbon content rises, while the magnesia content diminishes. Consulting the SEM images of the line scan, this could be due to a quarried out magnesia grain, leaving a carbon rich matrix.

The laboratory sample suffered more during the corrosion testing, as it lost about one third of its body (Fig. 11). It is also evident that some of the magnesia dropped out of the SiC structure, leaving big cavities. This may have happened during the dry cutting of the samples or during the test itself. The composition of the laboratory sample after the corrosion testing is shown in Fig. 12b. As expected from the pictures, the slag, namely the calcium, penetrated deeply into the structure. As the laboratory sample was embedded in an organic substance, carbon is not plotted as it is not possible to distinguish between carbon from the sample and carbon from the resin.

4.3.3 Numerical thermal shock experiments

In the numerical experiments, the maximal principal stress after the quasi-static heating and after the thermal shock loading is computed and linked with the microstructure (cf. Fig. 13). Since a linear elastic model was chosen, the maximal occurring stresses were used as failure criterion. According to Tab. 1, tensile stresses are significantly more critical for carbon and periclase than compressive stresses are. Hence, the maximal occurring stresses are compared with the fracture stresses of vitreous carbon and periclase.

Fig. 13a outlines the stress distribution in a pore-free MgO–C foam and a pore-free MgO–C brick in a depth of 3 mm underneath the surface, where the thermal loading was applied. Regardless of the microstructure, compressive stresses are mainly concentrated in the periclase phase, whereas tensile stresses occur predominantly in the carbon

Tab. 2 Modulus of Rupture (MOR), Cold Crushing Strength (CCS), and Hot Modulus of Rupture (HMOR) of laboratory and reference samples

	MOR [MPa]	CCS [MPa]	HMOR [MPa]
MgO–SiC	1,15 ± 0,44	1,02 ± 0,38	2,00 ± 0,88
Reference sample	13,10 ± 0,36	47,00 ± 0.89	3,84 ± 0,29
Reference sample (aged)	3,17	19,8	2,39

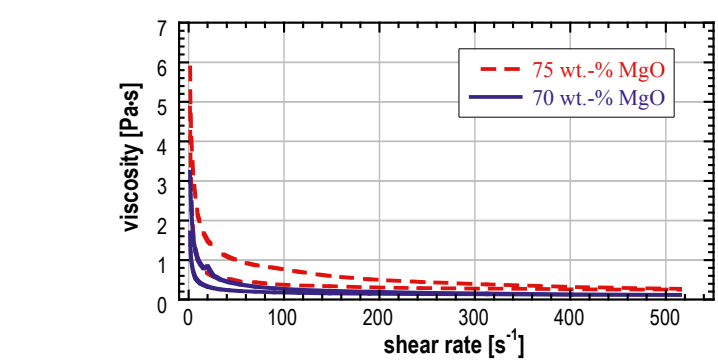

Fig. 9 Rheological behaviour of MgO slurries with different solid content

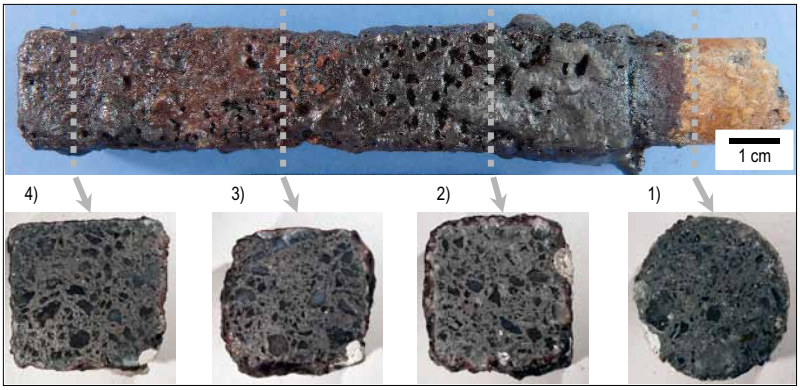

Fig. 10 Cross sections of the reference sample after the corrosion testing; the bar was fixed on the right side

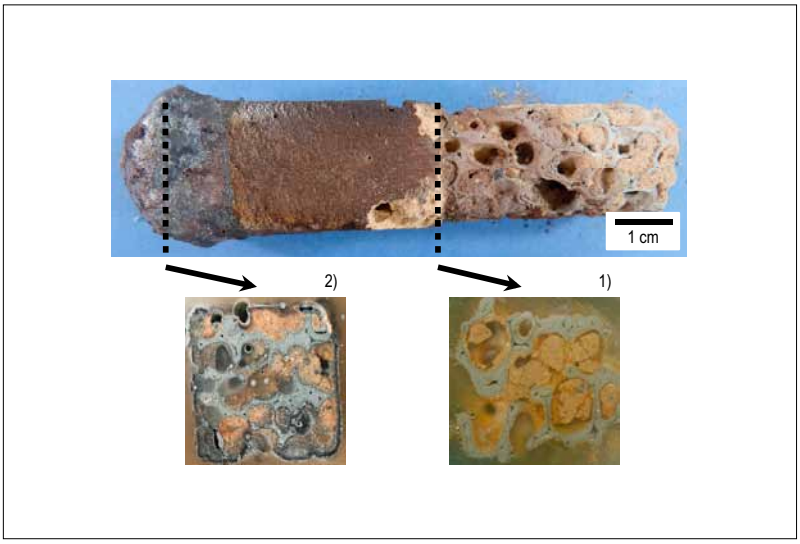

Fig. 11 Cross sections of the MgO–SiC laboratory sample after the corrosion testing; the bar was fixed on the right side

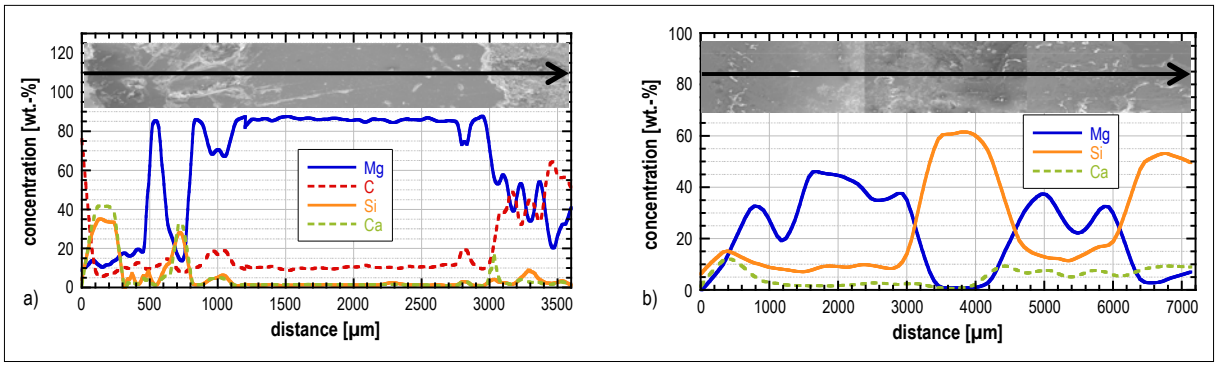

Fig. 12 a) Line scan of the reference sample (section 2) in Fig. 10; b) Line scan of the laboratory MgO–SiC sample (section 2) in Fig. 11

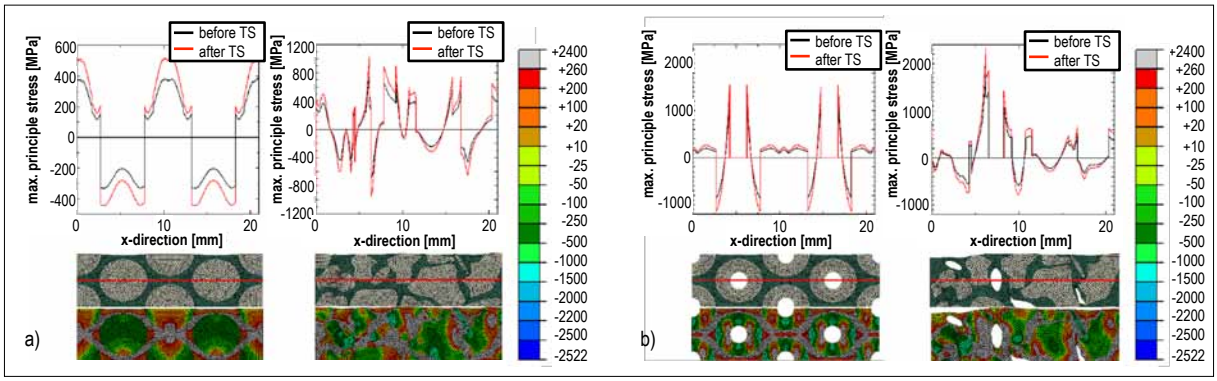

Fig. 13 a) Stress distribution in the microstructure of a MgO–C foam (l.), and of a MgO–C brick (r.) before and after Thermal Shock (TS): maximal principal stress (top), microstructure (middle) and contour plot after thermal shock (bottom); b) same for MgO–C containing air-filled pores

phase. Since the tensile stresses are critical for both phases, damage will mainly be concentrated in the carbon phase. The stresses before the thermal shock are related to permanent thermal stresses caused by the quasi-static heating due to the difference in the CTEs of carbon and periclase. For both microstructures, these stresses are lower than the stresses after the thermal shock. This kind of stress is caused by temporary thermal stresses due to the evolution of large temperature gradients in the MgO–C composite material. For both microstructures, the stress increase after the thermal shock in comparison to the stress state after the quasi-static heating is much more pronounced for the carbon phase than for periclase.

A comparison between cellular structure and conventional random brick outlines large stress peaks for the brick microstructure. These stress peaks are mainly concentrated at the interphase between MgO and carbon. The cellular MgO–C foams provide a periodical stress distribution with significantly reduced stresses in comparison to the brick structure. Nevertheless, as seen from the grey coloured regions in the contour plots in Fig. 13a that outline the damaged areas, for both microstructures, at some areas in the RVE, the actual stresses are above the tensile fracture stresses of MgO and carbon. As a result of the simplified used FE model of linear thermo-elasticity without damage, the damaged areas in the RVE structures will be overestimated.

In a second numerical study, the effect of air filled pores in both structures was investigated. Fig. 13b shows the stress distribution in a depth of 3 mm underneath the top surface in a MgO–C foam and a MgO–C brick with an air content of 10 %. Similar to the pore-free microstructures, the randomly distributed brick outlines much larger stresses than the periodic foam structure. There are significant stress peaks at the periclase/air interface. These are more than twice the stresses as in the pore-free structure. As a result, in comparison to the pore-free RVEs, a larger amount of the structure is damaged.

5 Conclusion

The main three constituents, foam struts, antioxidative interphase and matrix, play important roles in the final (thermo-)mechanical and high temperature corrosion properties of cellular magnesia/carbon composites. Even though, colloidal processing of cellular magnesia/carbon composites is an effective approach for manipulating strut-interphase-matrix microstructures, MgO hydration, drying shrinkage and sintering shrinkage have a crucial influence on density, residual porosity and pore size distributions of cellular refractory composites. Provided that the pore spaces are completely filled by advanced slurry infiltration, advanced (thermo-)mechanical characteristics of cellular magnesia/carbon refractories are expected. For this reason, obstacles to the controlled densification of cellular MgO/C composites remain and need to be resolved. The finite element analysis using a thermo-elastic model has been performed in order to investigate the structure-property relation of thermal damage in MgO–C refractories. Therefore, periodic cellular structures and random brick structures have been compared. The simulations show that tensile stresses are concentrated in the carbon phase, whereas compressive stresses

mainly occur in the periclase phase. It has been shown that under quasi-static heating and under thermal shock loading the periodic cellular microstructure leads to much lower stresses than in the common MgO–C brick structure. Furthermore, in order to reduce thermal damage, pore-free structures are to be preferred. As a result of the only elastic character of the model, lacking a real damage criterion, occurring stresses in the microstructure cannot be reduced by crack initiation and increasing crack density, hence the applied model overestimates the real situation for the thermal shock experiments. Nevertheless, the simplified model makes it possible to qualitatively predict the behaviour of refractories with a microstructure and to give first hints for the real experimental optimization of the microstructure.

Acknowledgement

The authors gratefully acknowledge the support and funding of the German Research Foundation – DFG grant no. FA 480/3-2 within the priority program DFG-SPP 1418 Refractories-Initiative to Reduce Emission – FIRE.

References

[1] Krass, Y. R.: World production of steel and magnesia refractories: State of the art and trends of development. Refract. Ind. Ceram **42** (2001) 417–425

[2] Damhof, F.; Brekelmans, W.A.M.; Geers, M.G.D.: Non-local modeling of thermal shock damage in refractory materials. Engin. Fract. Mech. **75** (2008) 4706–4720

[3] Damhof, F.; Brekelmans, W.A.M.; Geers, M.G.D.: Experimental analysis of the evolution of thermal shock damage using transit time measurement of ultrasonic waves. J. Europ. Ceram. Soc. **29** (2009) 1309–1322

[4] Falk, G.; et al.: Experimental characterization and thermo-mechanical modelling of micro structure interactions in cellular carbon magnesia refractories. J. of Ceramic Sci. and Technol. **5** (2014) 101–114

[5] Falk, G.; et al.: Feuerfeste MgO-C Komposite mit zellularer Kohlenstoffstruktur, Teil 1: Experimentelle Charakterisierung. Keram. Z. **4** (2014) 221–225

[6] Jung, A.; et al.: Thermal shock resistivity of hybrid carbon foam materials: Experimental and model predictions. Mech. Mater. **82** (2015) 13–27

[7] Jung, A.; et al.: Feuerfeste MgO-C Komposite mit zellularer Kohlenstoffstruktur. Teil 2: Mikrostrukturoptimierung durch thermo-mechanische Simulation. Keram. Z. **5/6** (2014) 295–300

[8] Kingery, W. D.: Factors effecting thermal stress resistance of ceramic materials. J. Amer. Ceram. Soc. **38** (1955) 3–17

[9] Hasselman, D.P.H.; Badaliance, R.; Chen, E.P.: Thermal fatigue and its failure prediction for brittle ceramics. In: Thermal Fatigue of Materials and Components, 1976, 55–67

[10] Hasselman, D.P.H.; et al.: Failure prediction of the thermal fatigue resistance of a glass. J. Mater. Sci. **11** (1976) 458–464

[11] Hasselman, D.P.H.: Rolle der Bruchzähigkeit bei der Temperaturwechselbeständigkeit feuerfester Erzeugnisse. Ber. DKG **54** (1977) 195–201

[12] Gruber, D.; Andreev, K.; Harmuth, H.: FEM simulation of the thermomechanical behaviour of the refractory lining of a blast furnace. J. Mater. Process. Technol. **155–156** (2004) 1539–1543

[13] Andreev, K.; Harmuth, H.: FEM simulation of the thermo-mechanical behaviour and failure of refractories – A case study. J. Mater. Process. Technol. **143–144** (2003) 72–77

[14] Stabler, J.; Baker, G.: Fractional step methods for thermo-mechanical damage analyses at transient elevated temperatures. Int. J. Numer. Methods Eng. **48 (**2000) 761–78

[15] Nechnech, W.; Meftah, F.; Reynouard, J. M.: An elasto-plastic damage model for plain concrete subjected to high temperatures. Engin. Struct. **24** (2002) 597–611

[16] Pearce, C.J.; et. al: Gradient enhanced thermo-mechanical damage model for concrete at high temperatures including transient thermal creep. Int. J. Numer. Anal. Methods Geomech. **28** (2004) 715–735

[17] Jung, A.; Diebels, S.: Thermo-mechanical properties of magnesia carbon foam composites. In: Coupled Problems in Science and Engineering VI, San Servolo, Venice, Italy, 2015, 94–105

[18] Damhof, F.; Brekelmans, W. A. M.; Geers, M. G. D.: Non-local modelling of cyclic thermal shock damage including parameter estimation. Eng. Fract. Mech. **78** (2011) 1846–1861

[19] Skiera, E.: Thermomechanische Charakterisierung neu entwickelter Feuerfestwerkstoffe. Jülich 2012

[20] Da Silveira, W.; Falk, G.: Reinforced cellular carbon matrix-MgO composites for high temperature applications: Microstructure aspects and colloidal processing. Adv. Engin. Mater. **13** (2011) 982–989

[21] Da Silveira, W. M.; Falk, G.: Production of refractory materials with cellular matrix by colloidal processing. refractories WORLDFORUM **4** (2012) 143–150

[22] Da Silveira, W.; Falk, G.: Functionalized cellular carbon-MgO composites: From interface processing to thermal shock resistant low-carbon MgO–C refractories. Adv. Engin. Mater. **16** (2014) 301–308

[23] Gaies, D.; Faber, K.T.: Thermal properties of pitch-derived graphite foam. Carbon **40** (2002) 1131–1150

[24] Chen, C.; et al.: Carbon foam derived from various precursors. Carbon **44** (2006) 1535–1543

[25] Li, S.; et al.: Formation mechanism of carbon foams derived from mesophase pitch. Carbon **49** (2011) 618–624

[26] Maleki, H.; et al.: Determining the shortest production time for glassy carbon ware. Carbon **35** (1997) 227–234

[27] Yarushina, T. V.; et al.: Periclase-carbon composite refractories with new complex binder. Refract. Ind. Ceram. **48** (2007) 170–175

[28] Lei, S.; et al.: Preparation of phenolic-based carbon foam with controllable pore structure and high compressive strength. Carbon **48** (2010) 2644–2673

[29] Oiye, É. N.; et al.: Development of an alternative route for production of glassy polymeric carbon electrodes in laboratorial scale. Macromol. Symp. 299–300 (2011) 147–155

[30] Inagaki, M.: New carbons-control of structure and functions. Amsterdam 2000

[31] Chen, Y.; et al.: Preparation of pitch-based carbon foam using polyurethane foam template. Carbon **45** (2007) 2126–2139

[32] Salomão, R.; Bittencourt, L. R. M.; Pandolfelli, V.C.: A novel approach for magnesia hydration assessment in refractory castables. Ceram. Int. **33** (2007) 803–810

[33] Amaral, L. F.; et al.: Chelants to inhibit magnesia (MgO) hydration. Ceram. Int. **37** (2011) 1537–1542

[34] Aneziris, C.; Dudczig, S., Helge, H.: Verfahren für die Herstellung von basischen kohlenstoffhaltigen Erzeugnissen durch Gießformgebung und/oder bildsame Formgebung. DE 102006031700 A1, 2008

[35] Noda, T.; Inagaki, M.; Yamada, S.: Glass-like carbons. J. Non-Cryst. Solids **1** (1969) 285–302

[36] Salmang, H., et al.: Keramik. Berlin, Heidelberg 2007